

We are IntechOpen, the world's leading publisher of Open Access books Built by scientists, for scientists

4,800

Open access books available

122,000

International authors and editors

135M

Downloads

Our authors are among the

154

Countries delivered to

TOP 1%

most cited scientists

12.2%

Contributors from top 500 universities



WEB OF SCIENCE™

Selection of our books indexed in the Book Citation Index
in Web of Science™ Core Collection (BKCI)

Interested in publishing with us?
Contact book.department@intechopen.com

Numbers displayed above are based on latest data collected.

For more information visit www.intechopen.com



Femtosecond Pulse Radiolysis

Jinfeng Yang, Koichi Kan, Masao Gohdo and Yoichi Yoshida

Abstract

Ultrafast pulse radiolysis with a short-pulsed electron beam and a short-pulsed analyzing light is a powerful time-resolved spectroscopic technique to study the kinetics and reactions of short-lived intermediate species or precursors in radiation chemistry and biology. In this chapter, first, we give an overview of historical developments of ultrafast pulse radiolysis. Then, we describe a femtosecond pulse radiolysis instrument, including the generation of femtosecond electron pulses by a photocathode radio frequency (rf) gun-based linear electron accelerator, the synchronization of femtosecond analyzing laser with the electron pulses, the transient absorption measurement with double-pulse technique, and the observations of the formation processes and ultrafast reactions of hydrated electrons in water. Finally, two innovative techniques, which enable to improve the time resolution in next pulse radiolysis development, are presented.

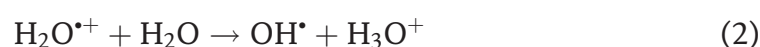
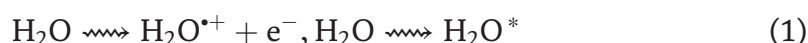
Keywords: pulse radiolysis, femtosecond electron pulse, femtosecond laser, short-lived intermediate species, precursors, hydrated electron, ultrafast reaction, radiation chemistry

1. Introduction

1.1 Primary processes in radiation chemistry

Primary processes or ultrafast reactions in radiation chemistry and biology are occurred in the ionization of molecules with radiation beams, for example, gamma- or X-rays, electrons, ions, and other high-energy particles. The ionization of molecules produces a positive radical ion and an electron with an initial kinetic energy. The electron will be thermalized by interactions with molecules, and then surrounded by solvent molecules to form solvated electron state in polar materials like water [1–3], or reacted with the positive radical ion by geminate recombination in nonpolar materials like alkenes [4–10].

For example, in water, the primary processes at the current state of knowledge in the radiation chemistry [11, 12] can be summarized as:



where Eq. (1) represents the ionization and electronic excitation of water molecules on a attosecond timescale ($\sim 10^{-16}$ s), Eq. (2) is the ion-molecular

reaction of positive radical ion $\text{H}_2\text{O}^{+\bullet}$ in $\sim 10^{-14}$ s, Eq. (3) is the dissociation of electronic excited state H_2O^* in $\sim 10^{-13}$ s, and Eq. (4) is the formation process of solvated electron (called also hydrated electron in water, denoted by e^-_{hyd}) in $\sim 10^{-13}$ s.

To study such ultrafast kinetics and reactions, two techniques have been developed: photolysis and pulse radiolysis. The photolysis is mainly used in photochemistry, while pulse radiolysis is widely used in radiation chemistry. In photolysis, short-lived intermediate species or precursors are produced by photoionization with high-energy photons or multiphoton excitation. The species and their reactions are measured by time-resolved absorption spectroscopy with analyzing laser light. The first observation of femtosecond solvation dynamics of hydrated electrons in water was achieved in 1987 by Migus et al. by photolysis with a femtosecond laser [1]. In pulse radiolysis, short-pulsed radiation, that is, pulsed X-rays, electrons, or ions, ionizes molecules. The short-lived intermediate species and primary processes are observed by transient absorption spectroscopy with an analyzing light. The first pulse radiolysis was developed in 1962 by Hart and Boag [13] using 1.8-MeV and 3- μs -long electron pulses generated by an electron accelerator. They succeeded firstly in the direct spectroscopic observation of the solvated electrons in aqueous solutions. The experimental results indicated that pulse radiolysis is a very promising technique to determine short-lived intermediate species or precursors and observe their kinetics or reactions.

1.2 Historical developments of ultrafast pulse radiolysis

Progress of particle accelerator technology plays a significant role in the ultrafast pulse radiolysis development. The first picosecond pulse radiolysis was developed at the University of Toronto in the late 1960s [14] using the fine structure of ~ 30 -ps electron pulse train with the duration of 30 ns generated by S-band (2856 MHz) linear electron accelerator (or linac). Cherenkov light emitted by the picosecond electron pulses was used as analyzing light to detect the transient absorption, as shown in **Figure 1**. However, in this pulse radiolysis, the sample was irradiated every 350 ps (one period of S-band microwave) by the electron pulse train. Reactions or kinetics with time constant of >350 ps overlapped in the measurement. To circumvent this problem, several picosecond pulse radiolysis facilities using picosecond single-pulse electron accelerators with a sub-harmonic bunching technique were constructed in 1970s and 1980s. Tabata et al. at the University of Tokyo developed a 20-ps pulse radiolysis with two parallel linacs [15–17]. One linac was used to generate a picosecond single-pulse electron beam to irradiate the sample.

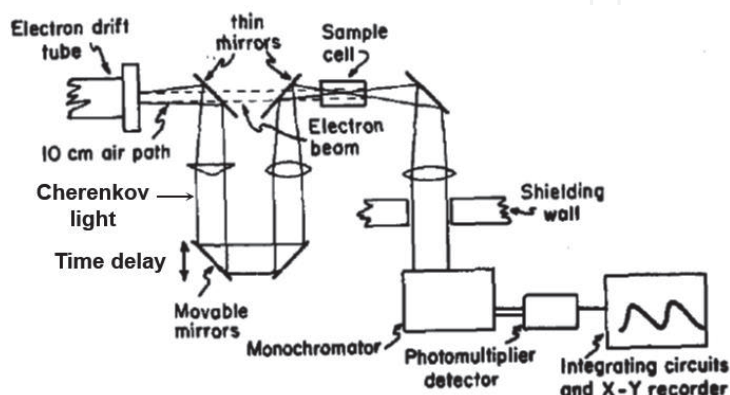


Figure 1.

First picosecond pulse radiolysis with time resolution of 23 ps developed at the University of Toronto in the late 1960s [14].

Another linac was used to produce picosecond single-pulse Cherenkov light. In 1990s, a picosecond pulse radiolysis system using the laser diode instead of the Cherenkov light was developed [18]. The system enabled to measure the transient absorption from the visible to near-infrared region. In the late 1990s, a femtosecond laser was used for the analyzing light to cover the wide wavelength range from ultraviolet to infrared [19]. However, in spite of many innovative techniques that have been developed, the time resolution had remained at ~ 20 ps since the 1970s.

A remarkable progress in ultrafast pulse radiolysis has been made since 2000. A sub-picosecond pulse radiolysis was developed at Osaka University using a sub-picosecond single-pulse electron beam and a femtosecond laser light [20]. The sub-picosecond single-pulse electron beam was generated by a 28-MeV L-band (1300 MHz) electron linac and a magnetic pulse compressor. A synchronized Ti:sapphire laser with pulse width of 60 fs was used as analyzing light source. Moreover, a time jitter compensation technique was developed by directly detecting the time interval between the electron pulse and the analyzing laser light with a femtosecond streak camera. Finally, the time resolution of 2 ps was achieved.

In the 2000s, a new type of ultrafast pulse radiolysis using an advanced accelerator technology of laser-triggered photocathode radio frequency (rf) electron gun was developed at the Brookhaven National Laboratory, at the University of Tokyo, at Sumitomo Heavy Industries, at the University of Paris-Sud, at Waseda University, and at Osaka University. The photocathode rf gun consists of two to four rf cavities driven with high rf power to accelerate the electrons emitted from the photocathode to an energy region of 4~9 MeV. The rf gun enables to generate a picosecond single-pulsed electron beam with electron charge of nano-coulombs using picosecond laser excitation on the photocathode. The new type of pulse radiolysis exhibits two crucial advantages: (1) the instrument is very compact without the need of the sub-harmonic bunching system and (2) the electron pulses produced by the rf gun are time-synchronized with laser pulses, resulting in a low time jitter between the electron pulse and the analyzing laser light. **Table 1** gives the ultrafast pulse radiolysis facilities using the photocathode rf guns.

In 2010, the first femtosecond pulse radiolysis with time resolution of 240 fs was successfully developed at Osaka University using a femtosecond single-pulsed electron beam generated by a 32-MeV photocathode rf gun linac and a magnetic pulse compressor [26–29]. The femtosecond pulse radiolysis was used successfully to observe the femtosecond solvation dynamics of hydrated electrons in water.

Facility	Instrument	Electron pulse characteristics	Refs.
Brookhaven National Laboratory	3.5-cell rf gun, ~ 100 -fs laser	≥ 7 ps, 6~8 nC, 8.7 MeV	[21]
University of Tokyo	1.6-cell rf gun, booster linac, 100-fs laser	7 ps, 0.65 nC, 18 MeV, time jitter: 2.1 ps	[22]
Sumitomo Heavy Industries	1.6-cell rf gun, 15-ps laser	20 ps, 1 nC, 1.75 MeV	[23]
University of Paris-Sud	1.5-cell rf gun, booster linac, 120-fs laser	< 5 ps, < 2 nC, 10 ps, 5 nC, 4~9 MeV	[24]
Waseda University	1.6-cell rf gun, 4.8-ps white light	6 ps, 1 nC, 4.5 MeV	[25]
Osaka University	1.6-cell rf gun, booster linac, 107-fs laser	98~400 fs, 0.1~1 nC, 32 MeV, time jitter: 61 fs	[26–29]

Table 1.
The ultrafast pulse radiolysis facilities using photocathode rf guns.

It paves the way to observe the short-lived intermediate species and primary processes in radiation chemistry on femtosecond timescale.

Recently, a technique of laser wakefield electron acceleration instead of the traditional accelerators was applied in ultrafast pulse radiolysis at the Argonne National Laboratory [30]. However, the time resolution is still limited to picosecond because of the electron pulse duration, the time jitter, and the effect due to group velocity mismatch (GVM) between the electron beam and the light in the sample.

In order to reduce furthermore the time jitter between the electron pulse and the analyzing light pulse, a technique of a “double-decker electron beam accelerator” was proposed in pulse radiolysis at Osaka University [31, 32]. The entirely synchronized double-decker electron beams with a time interval of 1.4 ns were generated in the photocathode rf gun with 2-ps laser beams, then accelerated to 32 MeV with a booster linac, and finally compressed into femtosecond with a magnetic compressor. One of the double-decker electron beams was used to irradiate the sample, while another beam was converted to the analyzing light, for example, Cherenkov light or terahertz (THz) light, resulting in the generation of entirely synchronized femtosecond-pulsed electron beam and femtosecond analyzing light. Moreover, in order to circumvent the effect of GVM, an innovative technique of “equivalent velocity spectroscopy (EVS)” was developed for pulse radiolysis at Osaka University [33]. The method of ultrafast pulse radiolysis was reviewed in a book entitled “Recent trends in radiation chemistry” edited by Wishart and Rao in 2010 [34].

In this chapter, we describe the details of femtosecond pulse radiolysis, including the generation of femtosecond electron pulses, the synchronization of femtosecond analyzing laser with the electron pulses, double-pulse technique for the transient absorption measurement, and the observations of formation processes and ultrafast reactions of hydrated electrons in water. Finally, two innovative techniques of EVS and double-decker electron beam accelerator will be introduced.

2. Femtosecond pulse radiolysis

Ultrafast pulse radiolysis is widely constructed with a stroboscopic method (a pump-and-probe method), as shown in **Figure 2**. The electron pulse is used as a radiation pulse, while the analyzing light pulse (laser or Cherenkov light) is used to measure the time evolution of transient absorption of short-lived intermediate species by changing the time interval between the electron pulse and the analyzing light pulse. In the stroboscopic method, the time resolution is determined by the electron pulse duration, the analyzing light pulse duration, and the time jitter between the electron pulse and the analyzing light pulse, as described in Section 3.1.

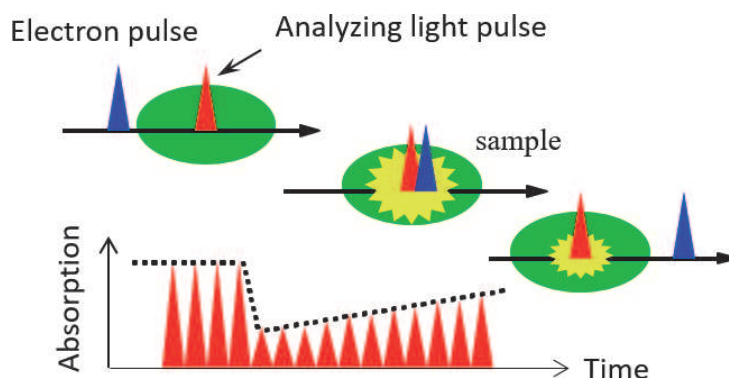


Figure 2. Schematic of stroboscopic method (pump-and-probe method) in ultrafast pulse radiolysis.

The progress of the ultrafast laser technology allows us to use a femtosecond laser as an analyzing light source in pulse radiolysis. However, in order to achieve a femtosecond time resolution, three significant techniques are indispensable:

1. generating a femtosecond-pulsed electron beam,
2. synchronizing the electron pulse with the analyzing light pulse in femtosecond, and
3. detecting the transient absorption with a good signal-to-noise (S/N) ratio in a thin sample cell to circumvent the effect of GVM.

In this section, we focus on the generation of femtosecond electron pulses with a laser photocathode electron gun accelerator, ultrafast pulse radiolysis with the femtosecond-pulsed electron beam and a femtosecond laser, and a double-pulse detection technique to observe the transient absorption in a thin sample cell.

2.1 1.6-cell photocathode rf gun

Femtosecond pulse radiolysis at Osaka University was constructed with a 1.6-cell S-band (2.856 GHz) photocathode rf gun, a booster linac, a magnetic pulse compressor, and an analyzing femtosecond Ti:sapphire laser, as shown in **Figure 3**.

The photocathode rf gun used in femtosecond pulse radiolysis contains two cavities: a half cell and a full cell. The length of the half-cell cavity was equal to 0.6

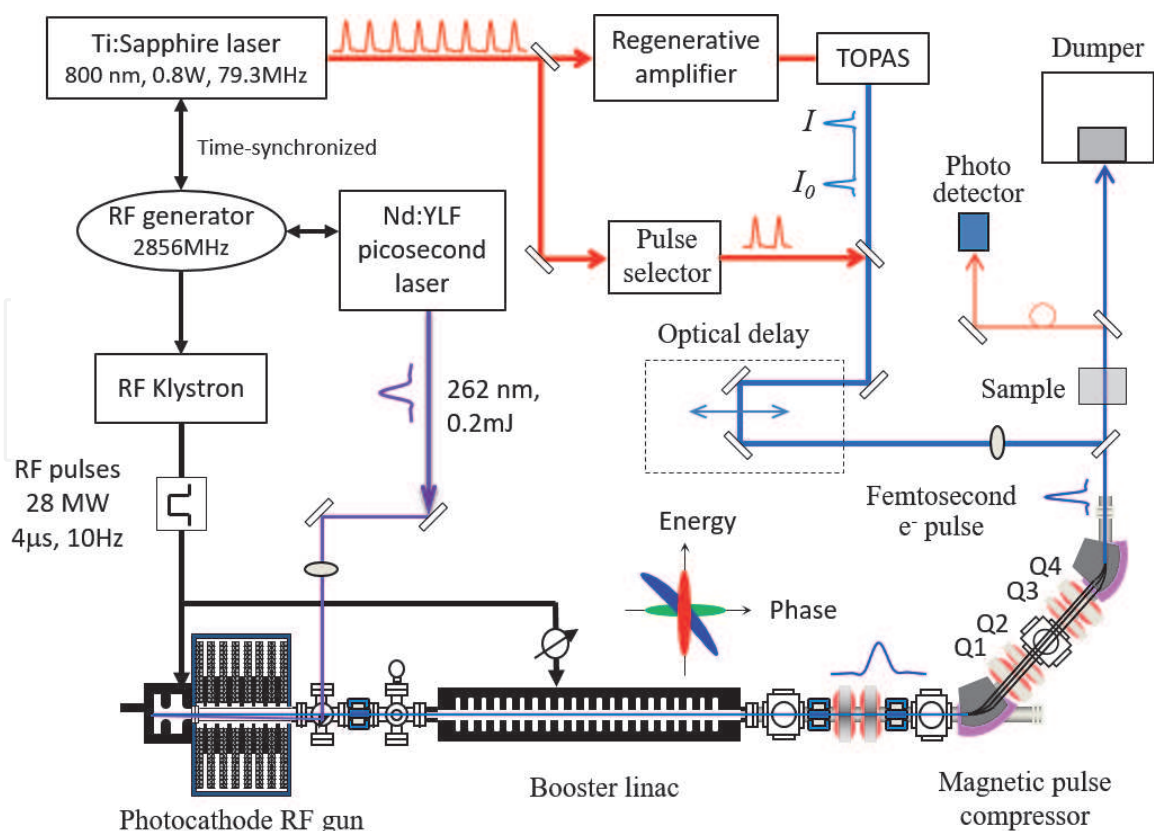


Figure 3. Schematic of femtosecond pulse radiolysis apparatus at Osaka University, containing a photocathode rf gun, a booster linac, a magnetic pulse compressor, and an analyzing femtosecond Ti:sapphire laser. The rf gun was driven by a picosecond Nd:YLF laser. A time resolution of 240 fs due to the electron beam and the analyzing laser has been achieved [26–29].

times $\lambda/2$ to minimize the beam emittance, while $\lambda = 104.96$ mm is the wavelength of 2.856-GHz rf. The cavities were operated with 10-MW peak rf power to produce a high-peak electric field of ~ 110 MV/m on photocathode and the cavities [35–39]. A copper cathode was used and illuminated by the fourth harmonic of Nd:YLF picosecond laser [262 nm, pulse duration: 5 ps in full width at half maximum (FWHM)], as described in Section 2.4. The incident angle of the laser light was approximately 2° along the electron beam direction using a mirror placed in vacuum. The laser injection phase (gun phase) was adjusted by changing the phase of the reference 79.3-MHz rf signal with a low-power phase shifter. A solenoid magnet was mounted at the exit of the rf gun to reduce the emittance growth due to the space charge effect during the propagation. The maximum magnetic field was 3 kG.

The characteristics of the electron beam generated by the rf gun are shown in **Table 2**. **Figure 4** gives the transverse emittance, pulse duration, and relative energy spread in root-mean-square (RMS) as a function of the laser injection phase. The rf gun enables to generate a low-emittance and low-energy-spread electron beam at the laser injection phase of $<40^\circ$. Moreover, the pulse compression inside the rf gun due to the rf effect occurred at $<40^\circ$, yielding a electron pulse duration less than that of the incident laser. However, the electron charge was decreased at a low laser injection phase, that is, 1.8 nC at 80° was decreased to 0.2 nC at 10° . In the pulse radiolysis experiment, the gun phase was fixed to 30° in the experiments.

Electron energy	4 MeV
Electron charge	1 nC/pulse
Pulse duration	1.8 ± 0.2 ps
Transverse emittance	3.2 ± 0.2 mm-mrad at 1 nC
Relative energy spread	0.05%
Repetition rate of pulses	10 Hz

Table 2.

The characteristics of picosecond electron beam generated by the rf gun at the laser injection phase of 30° [35].

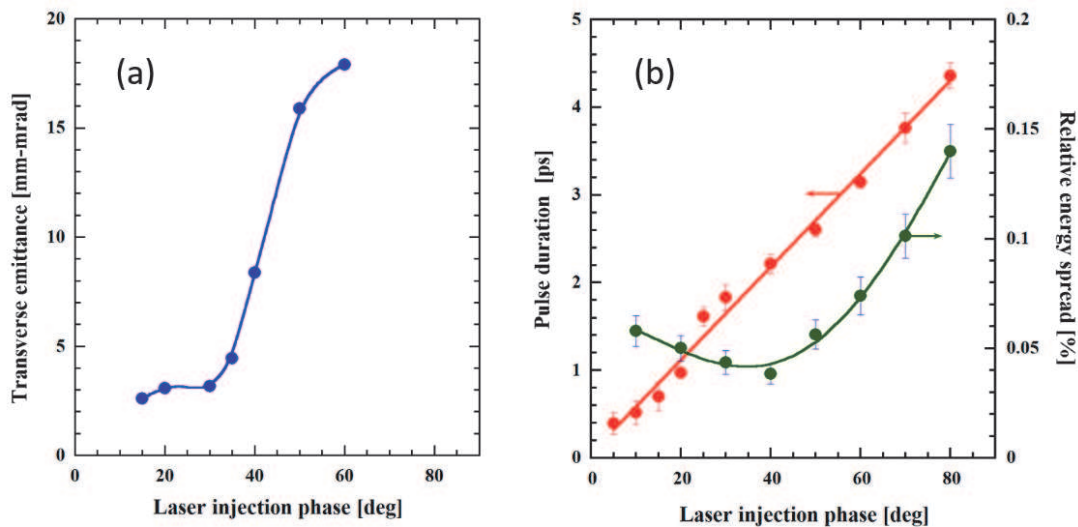


Figure 4.

The transverse emittance, pulse duration, and relative energy spread as a function of the laser injection phase [35]. The electron charge was 1.8 nC at 80° and was decreased to 0.2 nC at 10° .

2.2 Booster linear accelerator

A 2-m-long S-band traveling-wave booster linac was mounted downstream of the rf gun and the solenoid magnet at a distance of 1.2 m from the photocathode. The booster linac was driven by rf pulses with peak power of 25 MW. The duration of the rf pulses was 4 μ s. The repetition rate of the pulses was 10 Hz. The booster linac accelerates the electron pulses and makes an optimum energy-phase correction for pulse compression, where the electrons in the front of pulse has more energy than the electrons in the back of pulse, as shown as the blue pulse in **Figure 3**. The rf phase of the booster linac was adjusted by a high-power phase shifter mounted in the 25-MW rf line. The energy of the electrons was 32 MeV after the booster linac.

2.3 Magnetic pulse compressor

The magnetic pulse compressor consists of two 45°-bending magnets and four quadrupole magnets. To obtain an ultrashort electron pulse, all magnets were carefully installed with the minimum lattice error to reduce the aberrations in the phase space distribution. The outside two quadrupole magnets (Q1 and Q4) have equal magnetic fields, while the inside two quadrupole magnets (Q3 and Q4) have equal magnetic fields. They provide the necessary path length dependence on the electron energy. The dispersion function is symmetric on the mid-plane of the compressor. When the picosecond electron pulse with an optimum energy-phase correction (blue pulse in **Figure 3**) passes the magnetic pulse compressor, the pulse is compressed into femtosecond by rotating the pulse in longitudinal phase space, as shown as red pulse in **Figure 3**. However, higher order momentum dispersion in the compressor, especially the second-order dispersion, causes a nonlinear deformation of the longitudinal phase space, yielding the increase of the final pulse duration. To minimize the nonlinear effects, a nonlinear energy correlation of the electron pulse (blue pulse in **Figure 3**) was introduced before the compression by re-phasing the booster linac to $>90^\circ$ with a curvature of the rf waveform. Finally, the correlation offsets the effects of the nonlinear path length in the magnetic compression to obtain a short electron pulse [28].

Figure 5(a) gives the compressed pulse duration and the relative energy spread as a function of the rf phase of the booster linac at 1 nC [28]. The data show that the shortest pulse duration of 400 ± 58 fs RMS was obtained at 94° . At this phase, the booster linac accelerates the electrons with a nonlinear energy-phase correlation. The pulse duration was decreased by decreasing the electron charge, that is, a 98-fs-long electron pulse at 0.17 nC.

2.4 Laser system

The laser system contains an all solid-state LD-pumped Nd:YLF picosecond laser (Time-Bandwidth) and a Ti:sapphire femtosecond laser (Spectra-Physics). The Nd:YLF picosecond laser was used to generate a picosecond electron beam in the rf gun. The laser consists of a 79.3-MHz passive mode-locked Nd:YLF laser oscillator, a regenerative amplifier, and a wavelength converter. The 79.3-MHz laser pulses were phase-locked with a reference 79.3-MHz rf signal, which was generated by dividing the accelerating 2.856-GHz rf by 1/36, by dynamically adjusting the laser cavity length with a semiconductor saturable absorber mirror (SESAM) and a timing stabilizer. A single laser pulse of the oscillator was captured and amplified to the pulse energy up to 1 mJ in the regenerative amplifier. The repetition rate of the amplified pulses was 10 Hz. The amplified laser pulses were converted to ultraviolet

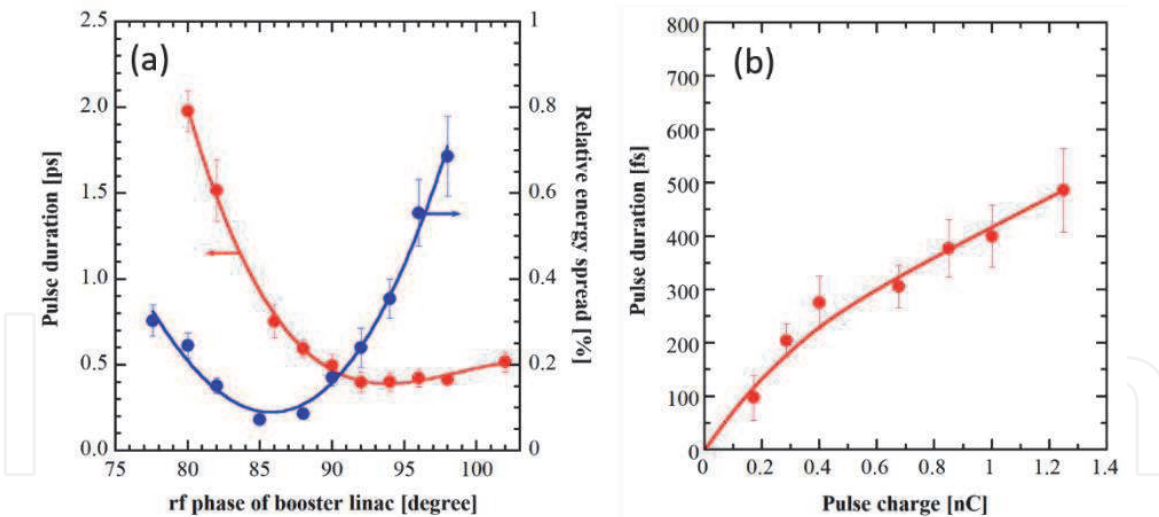


Figure 5.

(a) The compressed pulse duration and the relative energy spread as a function of the rf phase of booster linac at 1 nC and (b) the compressed pulse duration as a function of electron charge at the rf phase of 94° [28]. Copyright 2006, with permission from Elsevier.

pulses (UV: 262 nm) using two nonlinear crystals and guided to the photocathode in the rf gun. The pulse duration of UV light was 5 ps FWHM. The maximum pulse energy was 300 μ J.

The mode-locked Ti:sapphire femtosecond laser (Spectra-Physics) was used as analyzing light source in pulse radiolysis. The laser consists of a 79.3-MHz femtosecond Ti:sapphire laser oscillator (Tsunami, central wavelength: 800 nm), a regenerative amplifier (Spitfire), and a tunable optical parametric amplifier with frequency mixer stages (TOPAS-Prime and NirUVis), as shown in **Figure 6(a)**. The 79.3-MHz laser pulses were synchronized to the external 79.3-MHz RF signal with a time-to-lock piezoelectric device. The time jitter between the laser pulse and 79.3-MHz rf phase was 61 fs RMS [26], being approximately equal to the time jitter between the electron pulse and the analyzing laser pulse. The laser oscillator output was fed to the regenerative amplifier for pulse stretching, amplification, and compression. The regenerative amplifier was driven by a green laser with a repetition rate of 1 kHz (Empower, wavelength: 532 nm, output: 15 W). The pulse energy of the amplifier output was 0.8 mJ. The pulse duration was ~ 100 fs after the pulse compression. The amplified femtosecond laser beam was inputted to the optical

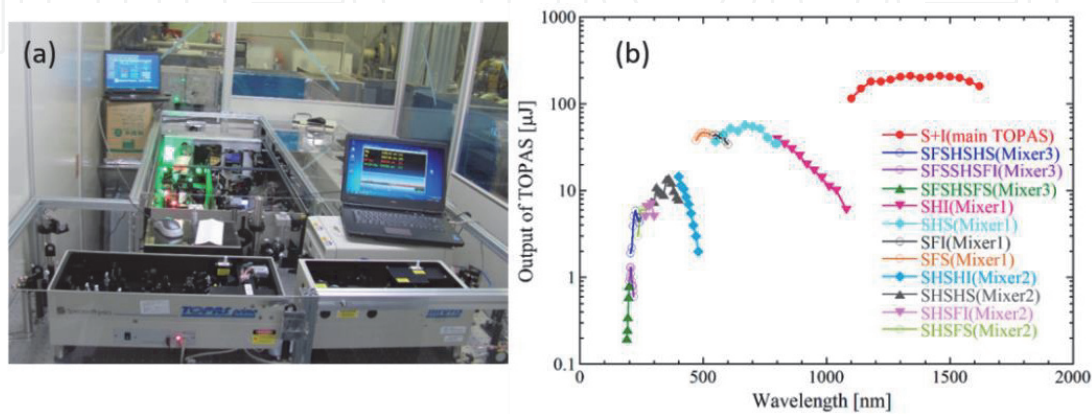


Figure 6.

(a) Photo of TOPAS-Prime and NirUVis and (b) the pulse energy of analyzing light as a function of wavelength, which facilitates pulse radiolysis [40]. Copyright 2017, with permission from Japan Radioisotope Association.

parametric amplifier to extend the tuning range into ultraviolet (UV), visible (VIS), or infrared (IR). **Figure 6(b)** shows the pulse energies of outputs of TOPAS-Prime and NirUVis [40]. An analyzing light with a wide wavelength range of 190~1600 nm facilitates pulse radiolysis based on the sample's requirements. The time delay between the electron pulse and the analyzing laser pulse was adjusted by changing the arrival time of the laser pulse at the sample with an optical delay.

2.5 Double-pulse technique: transient absorption measurement

Progress in the photodiode technology allows us to easily detect the transient absorption of intermediate species over a wide wavelength range from ultraviolet to infrared, that is, using silicon photodetectors in wavelength range from 200 to 1000 nm (PDA10A, Thorlabs) and InGaAs photodetectors in wavelength range from 800 to 1700 nm (PDA10C, Thorlabs). However, the development of transient absorption detection technique with a good S/N ratio is very significant in ultrafast pulse radiolysis, especially for the use of low-charge femtosecond electron pulses and a thin sample cell to circumvent the effect of GVM.

For this purpose, we developed a double-pulse measurement technique to reduce the fluctuation of the laser intensity caused by long-term drift and mechanical vibration of optics. **Figure 7** shows the concept of the double-pulse measurement. Two analyzing laser pulses with a time interval of Δt are incident on the sample. The front laser pulse is used as “reference pulse” before the electron irradiation, while the back laser pulse is used as a “signal pulse” to measure the absorption after the electron irradiation. The optical density is thus obtained by

$$OD = \log \frac{I_0}{I} \quad (5)$$

where I_0 and I are the signals of the reference and signal pulses detected by a photodiode, respectively. The time interval between two pulses was $\Delta t = 1$ ms using the outputs of the optical parametric amplifier.

The output of the Ti:sapphire laser oscillator (Tsunami) with the wavelength of 800 nm was also utilized in pulse radiolysis [29]. The continuous pulses of 79.3 MHz were guided to a pulse selector (Spectra-Physics, 3980), which was constructed with an Acousto-Optic Modulator (AOM) crystal driven by the 79.3-MHz rf pulses. The selector extracted a pulse train containing several pulses by adjusting the rf pulse duration and phase. Finally, two stable pulses of the pulse train with a same

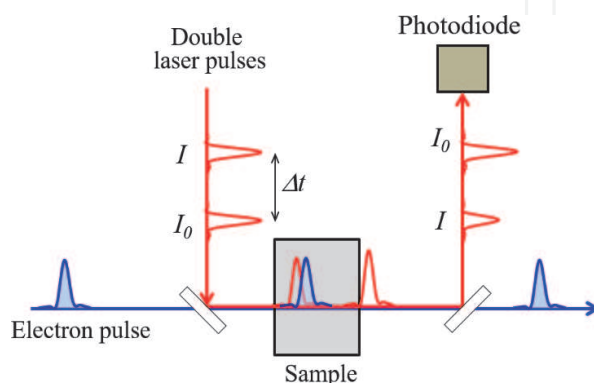


Figure 7. Schematic of double-pulse measurement in pulse radiolysis to reduce the fluctuation of the laser intensity caused by long-term drift and mechanical vibration of optics.

intensity were used as the double-pulse measurement. The time interval between two pulses was $\Delta t = 12.6$ ns. The previous studies [26, 27] indicate that this technique enables to detect a small optical density of 0.001 with an acceptable S/N ratio in a thin sample cell with optical length of 0.18 mm.

3. Pulse radiolysis experiments

3.1 Observations of solvation dynamics of hydrated electrons in water

In order to reduce the degradation of time resolution due to GVM, a thin sample cell with an optical length of 0.18 mm was used in the observation of hydrated electrons [26]. The water sample was deionized and Ar-saturated before the measurement. The double pulses with time interval of 12.6 ns generated by the 79.3-MHz Ti:sapphire laser oscillator and the pulse selector were used as analyzing light. The wavelength was 800 nm with a bandwidth of 12.5 nm FWHM. The pulse energy was approximately 10 nJ. The duration of the laser pulses was 107 fs RMS. The intensities of the reference pulse and the signal pulse were detected by a silicon photodiode and a digital phosphor oscilloscope. A femtosecond electron beam with pulse duration of 201 fs RMS at 0.4 nC generated by the accelerator system was used to irradiate the sample. The time jitter between the laser pulse and the electron pulse was measured to 61 fs RMS.

Figure 8 shows the first observation of ultrafast transient absorption kinetics of hydrated and pre-hydrated electrons in water pulse radiolysis. The transient absorption kinetics of pre-hydrated electrons were observed in a water sample cell with an optical length of 1 mm at the wavelength of 1300 nm. The kinetics observed in **Figure 8(a)** are in agreement with the formation process of hydrated electrons in the multiphoton ionization with two-state model, in which the hydrated electron is formed via a short-lived precursor (called “pre-hydrated electron,” denoted by e^-_{pre}) as

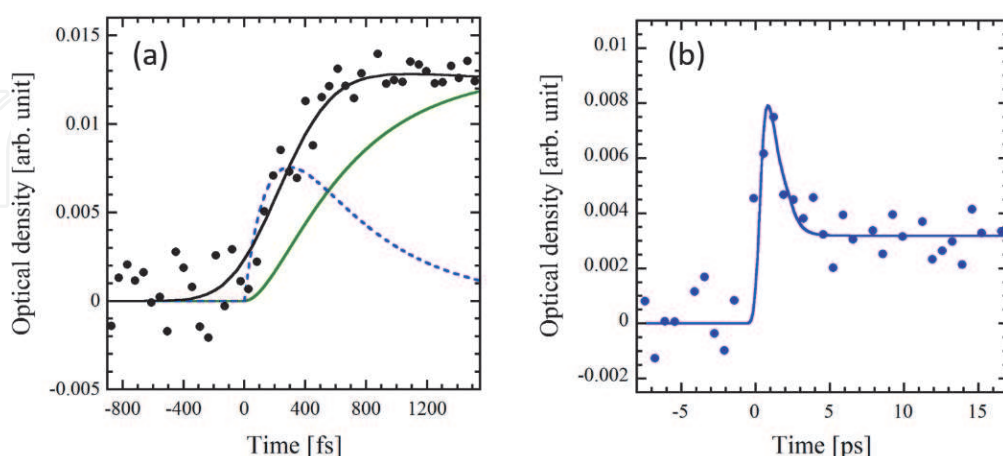


Figure 8.

(a) Femtosecond transient absorption kinetics of hydrated electrons observed in a thin water sample with an optical length of 0.18 mm at the wavelength of 800 nm, and (b) picosecond transient absorption kinetics of pre-hydrated electrons observed in a water sample cell with an optical length of 1 mm at the wavelength of 1300 nm. The blue and green lines in **Figure 8(a)** show the decay of pre-hydrated electrons and the formation of hydrated electrons with a time constant of 550 fs. The black line represents the kinetics of reaction (6) with $\tau_1 = 180$ fs and $\tau_2 = 550 \pm 50$ fs. The data at ≤ 3 ps in **Figure 8(b)** are mainly contributed by the pre-hydrated electrons, while the data at > 3 ps represent the kinetics of hydrated electrons with a long time decay. Copyright 2017, with permission from Japan Radioisotope Association.

where e^-_{th} represents the thermalized electron. When we fit the data in **Figure 8(a)** with the reaction (6), we found that the hydrated electrons are formed by the decay of pre-hydrated electrons with a time constant of $\tau_2 = 550 \pm 50$ fs and the pre-hydrated electrons are formed within $\tau_1 = 110 \sim 200$ fs after the electron irradiation. The obtained formation time of hydrated electrons in water pulse radiolysis is in agreement with that of $\tau_1 = 540$ fs obtained in multiphoton ionization studies [2, 3].

The time resolution of pulse radiolysis based on the stroboscopic method can be estimated by two components: one is the time resolution due to the electron beam and the analyzing laser light, and another is the time resolution due to GVM in the sample. The time resolution due to the electron beam and the laser light can be estimated by

$$\delta t_b = \sqrt{\sigma_e^2 + \sigma_l^2 + \sigma_j^2} \quad (7)$$

where $\sigma_e = 201$ fs RMS is the electron pulse duration, $\sigma_l = 107$ fs RMS is the analyzing laser pulse duration, and $\sigma_j = 61$ fs RMS is the time jitter between the two pulses, yielding $\delta t_b = 240$ fs.

The time resolution due to GVM in the sample with the experimental setup as shown in **Figure 7** can be calculated by

$$g(L) = L \left(\frac{n}{c} - \frac{1}{v} \right) \quad (8)$$

where $L = 0.18$ mm is the optical length of the sample, n is the refractive index of the sample, $n = 1.33$ for water sample, c is the velocity of light in vacuum, and v is the velocity of the electrons ($v \cong c$ for the 32-MeV electrons), yielding $g(L) = 198$ fs. Therefore, the total resolution of pulse radiation was $\Delta\tau = \delta t_b + g(L) = 438$ fs, which is available to observe the formation process of hydrated electrons with a time constant of 550 ± 50 fs in water as shown in **Figure 8**.

3.2 Observations of ultrafast spur reactions in water pulse radiolysis

Although the formation time of hydrated electrons in pulse radiolysis is similar to that in the multiphoton ionization, the thermalization distance (length of initial distribution) of electrons in pulse radiolysis is longer than that in the photoionization because the electrons produced by radiation ionization have a high initial kinetic energy. It causes some difference of spur reactions (primary processes) in the early time, containing the reactions of hydrated electrons with H_3O^+ cation and OH^\bullet radical pair:



Figure 9 shows the time evolution of hydrated electrons observed in water pulse radiolysis at 800 nm [40] and obtained in photolysis with a photoexcitation energy of 8.3 eV [41]. The data show that a small magnitude ($\sim 10\%$) of the hydrated electrons decreases in the first 40 ps due to the spur reactions (reactions (9) and (10)) in pulse radiolysis, while 38% of hydrated electrons reacted with H_3O^+ cation and OH^\bullet radical pair in photolysis with a photoexcitation energy of 8.3 eV. We fit the data by a numerical calculation of the survival probability of the hydrated electrons in the reactions (9) and (10) with a Gaussian initial distribution of hydrated electrons in water as in the photolysis study [41]:

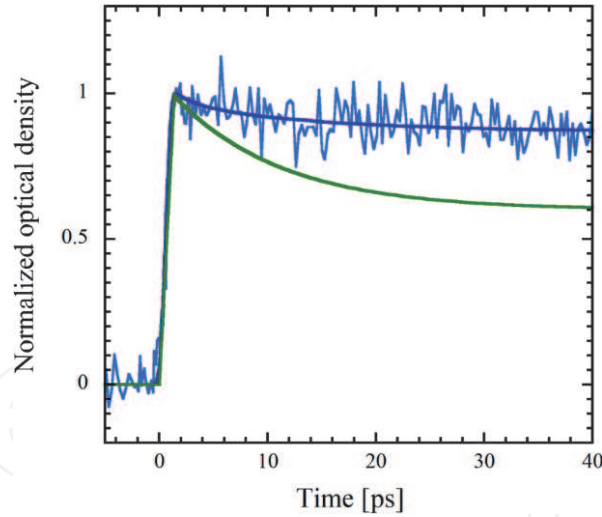


Figure 9.

Time evolution of hydrated electrons observed in water pulse radiolysis at 800 nm (blue lines) and in photolysis with a photoexcitation energy of 8.3 eV (green line) [41]. Copyright 2017, with permission from Japan Radioisotope Association.

$$f(r_0) = \frac{1}{\sqrt{8\pi^3\sigma^6}} \exp\left(-\frac{r_0^2}{2\sigma^2}\right), \quad \text{and} \quad \langle r_0 \rangle = \sigma\sqrt{8/\pi} \quad (11)$$

where $\langle r_0 \rangle$ is the distance of the hydrated electron distribution (the average thermalization distance). We found $\langle r_0 \rangle = 7\sim 9$ nm in pulse radiolysis, which is much longer than $\langle r_0 \rangle = 0.9$ nm in the photolysis with a photoexcitation energy of 8.3 eV. The long distance in water pulse radiolysis causes a small magnitude of the hydrated electrons reacting with H_3O^+ cation and OH^\bullet radical pair in the first 40 ps.

The raw data in **Figure 9** give the ratio of optical density at 1.5 and 20ps, $\text{OD}_{1.5\text{ps}}/\text{OD}_{20\text{ps}} = 1.12$. Using a hydrated electron yield (G-value) of 4.1 per 100 eV obtained at 20ps in previous water pulse radiolysis studies [21, 22], we then obtained $G = 4.6 \pm 0.3$ at 1.5ps, which is as good as the initial yield of hydrated electrons in water pulse radiolysis because the thermalized electrons are fully hydrated at 1.5ps. The obtained G-value is in agreement with the initial yield of 4.8 estimated in scavenger studies [42].

3.3 Equivalent velocity spectroscopy

The degradation of time resolution due to GVM in the sample can be reduced using a thin sample cell. However, the use of thin sample cell leads to a small absorption signal (optical intensity) and the degradation of S/N ratio in the measurement. On the other hand, due to the space charge effect, the ultrashort electron pulses are realized only at low electron charge, that is, sub-20-fs electron pulses at 2.1 pC [39]. Therefore, the increase of both the time resolution and the absorption signal is a great challenge in pulse radiolysis.

To circumvent the GVM problem and increase the absorption signal, we proposed an innovative technique of equivalent velocity spectroscopy (EVS) in pulse radiolysis [33]. The approach of EVS is shown in **Figure 10**. The electron pulse and the analyzing laser pulse are incident on the sample with an angle (θ) determined by the refractive index (n) of the sample as $\cos\theta = 1/n$. If we rotate the electron pulse with an angle (φ) and $\varphi = \theta$, both the rotated electron pulse and the analyzing light pulse precisely overlap at every point in the sample, resulting in the entire circumvention of GVM between the electron beam and the light in the sample.

In EVS, the time resolution due to GVM in the sample can be thus calculated by

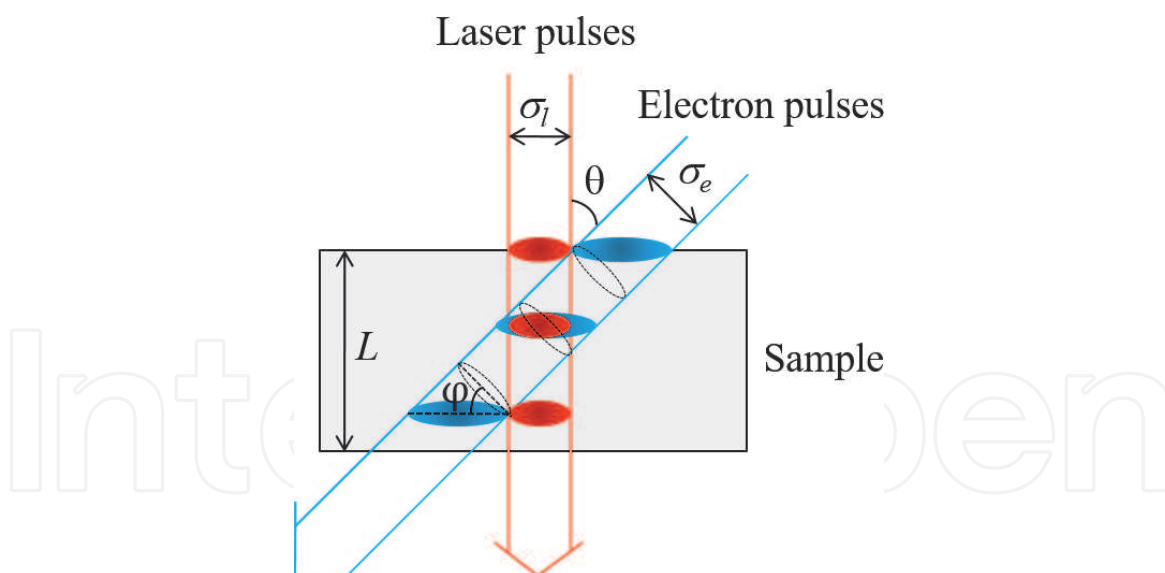


Figure 10. Schematic of EVS in pulse radiolysis with rotated electron pulses and analyzing laser pulses [33]. Copyright 2009, with permission from Elsevier.

$$g(L) = \sigma_e \left(\frac{\sin\varphi}{v_e \cos\varphi} + \frac{\cos\theta}{v_e \sin\theta} - \frac{1}{v_l \sin\theta} \right) + \sigma_l \left(\frac{1}{v_e \sin\theta} - \frac{\cos\theta}{v_l \sin\theta} \right) \text{ for } L > \frac{\sigma_l \cos\theta}{\sin\theta} + \frac{\sigma_e}{\sin\theta}, \quad (12)$$

where σ_e and σ_l are the sizes of the electron beam and the analyzing light respectively, φ is the rotation angle of the electron pulse, v_e and v_l are the velocities of the electrons and the analyzing light in the sample respectively, with $\approx c$ for the 32-MeV electrons and $v_l = c/n$. If $\varphi = \theta$ in Eq. (12), $g(L) = 0$. It means that the resolution limitation due to GVM in the sample is thus fully removed. Moreover, a long optical length (L) can be used in EVS.

The technique of the electron pulse rotation is very significant in EVS. In order to rotate the electron pulse, first, we adjusted the accelerating rf phase in the booster linac to increase the relative energy spread in the electron pulse, shown as the red pulse at the exit of the linac in **Figure 11(a)**. Then, we transported the electron pulse through the magnetic pulse compressor. The electron pulse was thus rotated along the propagation direction, shown as the red pulse at the exit of the compressor in **Figure 11(a)**. The rotation angle increased by increasing the accelerating rf phase in the booster linac. **Figure 11(b)** shows the 2D images of the electron pulses with different rotation angle at exit of the pulse compressor measured by a femtosecond streak camera at the accelerating rf phase of $\varphi_{rf} = 94^\circ$, 99° , and 103° [33]. The electron charge was 1.8 nC per pulse. At $\varphi_{rf} = 94^\circ$, an optimal energy-phase correlation in the electron pulse was produced for the bunch compressor, as described in Section 2.3. The electron pulse was compressed into the shortest pulse duration of 2 ps FWHM or 0.8 ps RMS, but the electron pulse was not rotated. At $\varphi_{rf} = 99^\circ$, the rotation angle of the electron pulse was $\varphi = 41^\circ$, which is a required angle for water sample. However, the pulse duration was increased to 5 ps. It was caused mainly by the large relative energy spread in the magnetic pulse compressor. At $\varphi_{rf} = 103^\circ$, $\varphi = 59^\circ$, and the pulse duration was increased to 6 ps.

In the demonstration of EVS, we measured the transient absorption kinetics of hydrated electrons in water using rotated electron pulses ($\varphi = 41^\circ$) and unrotated electron pulses ($\varphi = 0^\circ$). A sample cell with an optical length of 10 mm was used. The electron beam and the analyzing light were incident on the sample with the angle of $\theta = 41^\circ$. The electron charge was 1.8 nC per pulse. The duration of the

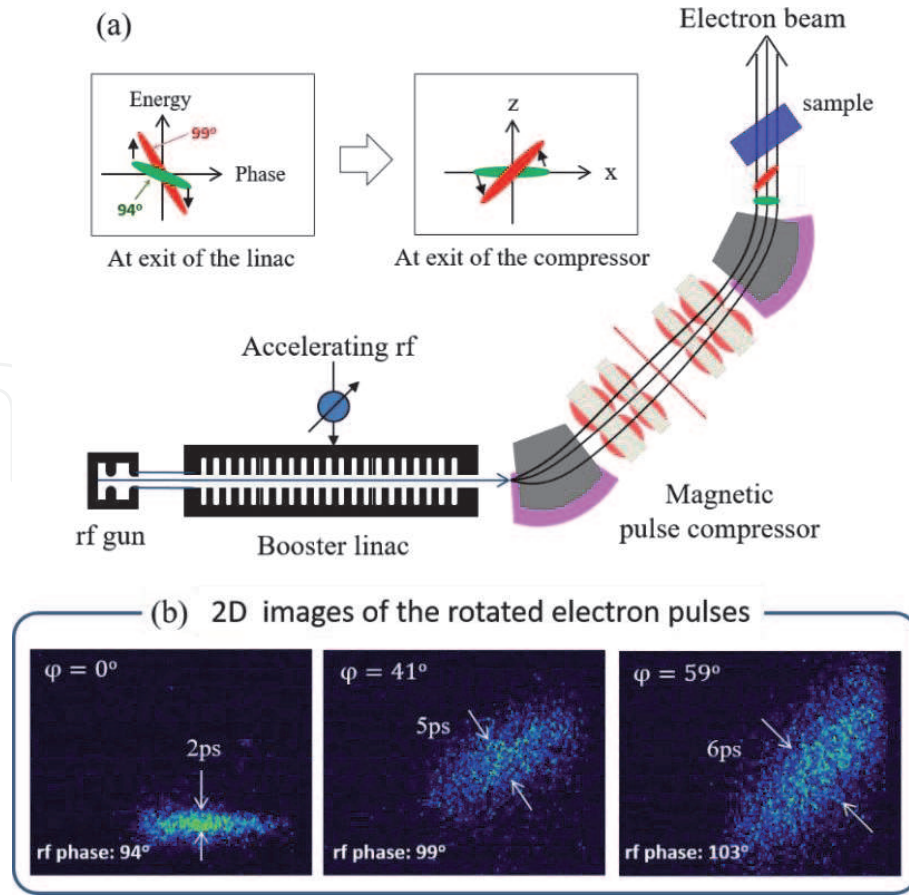


Figure 11. (a) Schematic of electron pulse rotation using the booster linac and magnetic pulse compressor. (b) 2D images of electron pulses with different rotation angle at exit of the pulse compressor measured by a femtosecond streak camera at the accelerating rf phase of $\phi_{rf} = 94^\circ$, 99° , and 103° [33]. Copyright 2009, with permission from Elsevier.

electron pulses was 2 ps at $\varphi = 0^\circ$ and 5 ps at $\varphi = 41^\circ$, as shown in **Figure 11(b)**. The double-pulse measurement with time interval of 12.6 ns, output of the 79.3-MHz Ti:sapphire laser oscillator, was used. The duration of the laser pulses was 107 fs RMS. The sizes of the electron beam and the analyzing laser light used in EVS were $\sigma_l = 2$ mm and $\sigma_e = 3$ mm, respectively.

Figure 12 gives the transient absorption kinetics of hydrated electrons in water measured by EVS. The rise time of the signals was 11.4 ps with the unrotated electron pulses and was reduced to 6.4 ps with the rotated electron pulses. A higher optical density was obtained with the rotated electron pulses. Under the experimental conditions, we calculated the time resolution due to GVM in the sample to $g(L) = 8.7$ ps using the unrotated electron pulses ($\varphi = 0^\circ$) and $g(L) = 0$ ps using the rotated electron pulses ($\varphi = 41^\circ$), according to Eq. (12). On the other hand, the time resolution due to the electron beam and the analyzing light was calculated in Eq. (7) to be $\delta t_b \cong 2$ ps for the unrotated electron pulses and $\delta t_b \cong 5$ ps for the rotated electron pulses. The total time resolution in EVS pulse radiolysis was estimated to be $\Delta\tau = 10.7$ ps using unrotated electron pulses and $\Delta\tau = 5$ ps using unrotated electron pulses, which are in a good agreement with the obtained rise time in the measurements using both the unrotated and rotated electron pulses.

The results indicate that (1) EVS is a very promising technique to circumvent the degradation of the time resolution due to GVM in the sample, and (2) higher optical densities can be obtained in EVS with the rotated electron pulses because two pulses overlap at every point in the sample and a thick sample can be used. However, the technique of the electron pulse rotation without the increase of the pulse duration remains to be developed.

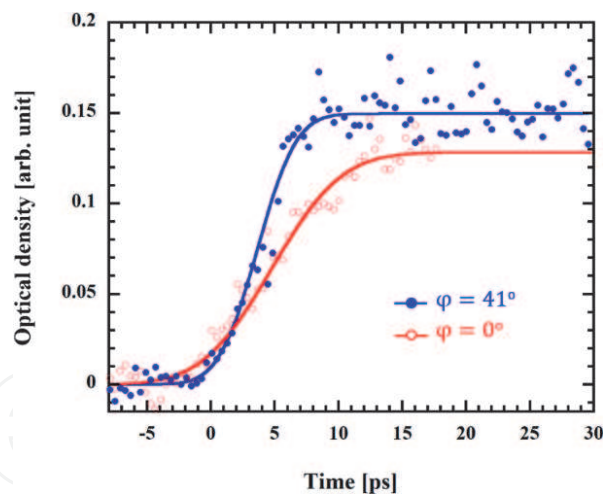


Figure 12.

Transient absorption kinetics of hydrated electrons in water measured in EVS pulse radiolysis with the rotated electron pulses (blue solid dots) and unrotated electron pulses (red circles) [33]. The wavelength of the analyzing laser light was 800 nm. Copyright 2009, with permission from Elsevier.

3.4 Double-decker electron beam accelerator

Recently, progress of the advanced particle accelerator and ultrashort laser technologies enables the generation of attosecond electron and laser pulses. When using such ultrashort electron and laser pulses in pulse radiolysis, the time jitter between the two pulses becomes a serious problem. Here, we introduce a technology of double-decker electron beam accelerator to generate both entirely synchronized electron pulse and analyzing light pulse for pulse radiolysis.

Figure 13 shows the concept of the double-decker electron beam accelerator for pulse radiolysis [31, 32]. The output of Nd:YLF picosecond laser was divided by a beam splitter to produce 2-ps laser beams with different positions in the vertical direction. The 2-ps laser beams were illuminated the photocathode in the rf gun. An optical delay was mounted in the up beam line to time delay the up beam. Two electron beams generated in the rf gun were accelerated in the booster linac up to 32 MeV and were then compressed into femtosecond with the magnetic pulse compressor.

Figure 13(b) shows the images of two electron beams with up and down positions at the exit of the compressor, which are called double-decker electron beams. In the experiment, the spot sizes of two laser beams on the photocathode were approximately 1 mm. The distance between the two beams was 2 mm in the vertical direction. The signals of the double-decker electron beams measured by a current transformer are shown in **Figure 13(c)**. The electron charges of double-decker beams were 0.47 nC per pulse (up-beam) and 0.65 nC per pulse (down beam). The different charges were due to the different pulse energies of two laser beams produced in the beam splitter. The time interval of the double-decker electron pulses was 1.4 ns, which is equal to four periods (4×0.35 ns) of the accelerating 2856-MHz rf. The double-decker electron beams have a low emittance of 2.5 ± 0.6 mm-mrad for the up beam and 3.6 ± 0.7 mm-mrad for the down beam, and a low relative energy spread of $0.14 \pm 0.03\%$ for both the beams. These enable to compress the double-decker pulses into femtosecond with the magnetic pulse compressor. **Figure 14** shows the temporal distributions of the double-decker electron pulses after the pulse compression measured by a femtosecond streak camera [31]. The pulse duration was obtained to 430 ± 25 fs FWHM for the up beam and 510 ± 20 fs FWHM for the down beam. The difference in the pulse duration for the double pulses was due to the different pulse charge. The two beams

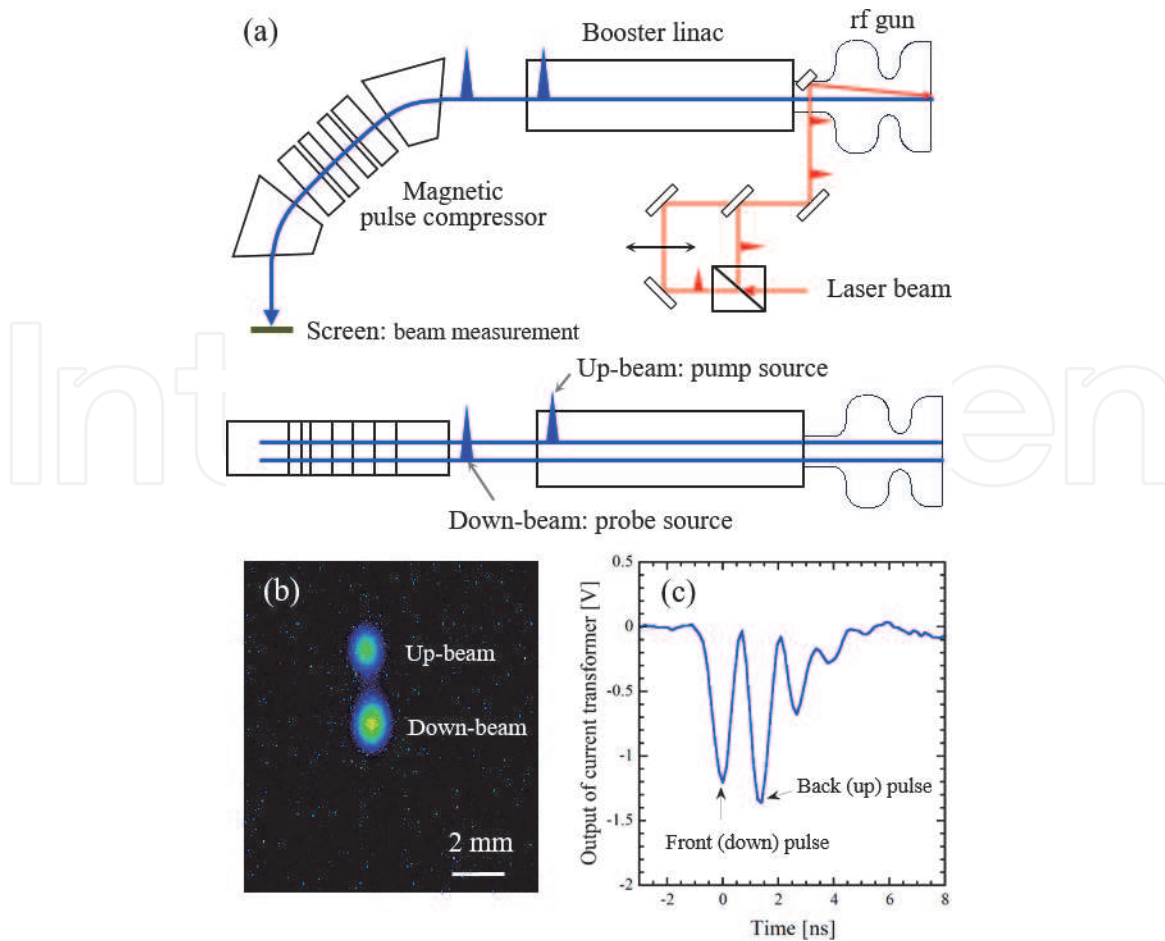


Figure 13. (a) Top view and side view of double-decker electron beam accelerator, (b) images and (c) signals of double-decker electron beams [31]. Copyright 2009, with permission from American Institute of Physics.

were generated by a laser and accelerated within an accelerating rf pulse. The theoretical estimation indicates that the time jitter in double-decker electron pulses can be reduced to attosecond by using a stable accelerating rf.

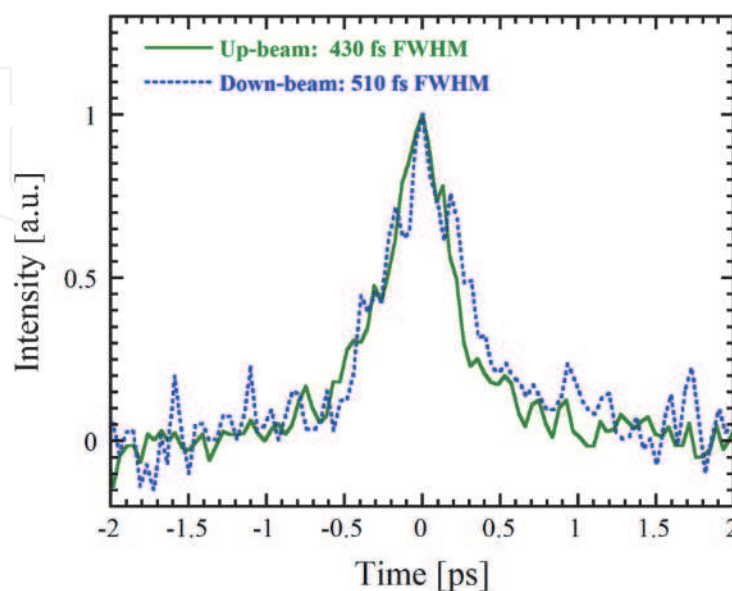


Figure 14. Temporal distributions of the double-decker electron pulses after the pulse compression measured by a femtosecond streak camera [31]. The pulse duration of the up beam was 430 ± 25 fs FWHM (green solid line), while the pulse duration of the down beam was 510 ± 20 fs FWHM (blue dashed line). Copyright 2009, with permission from American Institute of Physics.

In pulse radiolysis, the front electron pulse was converted to the femtosecond analyzing light with Cherenkov radiation, while the back electron pulse irradiated the sample. A band-pass filter was used to select a necessary wavelength for measurement. An optical delay was used to change the time delay between the Cherenkov light pulse and the irradiating electron pulse. In the demonstration, we succeeded to observe the time evolution and spectrum of transient absorption of hydrated electrons in water [32].

4. Conclusion

In this chapter, we introduced a femtosecond pulse radiolysis instrument, including the generation of femtosecond electron pulses, synchronization of femtosecond analyzing light with the electron pulses, a technique of double-pulse measurement to improve S/N ratio, and the first observation of femtosecond formation processes of hydrated electrons in water. A time resolution of 240 fs due to the electron beam and the analyzing laser has been achieved [26–29]. The femtosecond pulse radiolysis enables the observation of the transient absorption in a thin sample cell with an optical length of 0.18 mm, and paves the way to observe the short-lived intermediate species and primary processes in radiation chemistry and biology on femtosecond timescale.


Two innovative techniques namely “equivalent velocity spectroscopy (EVS)” and “double-decker electron beam accelerator” were presented for next pulse radiolysis development. EVS enables to circumvent entirety the effect of group velocity mismatch (GVM) between the electron beam and the analyzing light in the sample. The double-decker electron beam technique can be expected to reduce the time jitter between the electron pulse and the light pulse to attosecond. Moreover, the double-decker electron beam accelerator enables to generate both ultrashort pulse electron beam and analyzing light. Of course, the electron pulse rotation without the increase of pulse duration and some other problems remain to be solved; however, a combination of the EVS technology with the double-decker electron beams enables the development of ultrafast pulse radiolysis with sub-femtosecond or attosecond time resolution to reveal the entire primary processes beginning ionization in radiation chemistry and biology.

Author details

Jinfeng Yang*, Koichi Kan, Masao Gohdo and Yoichi Yoshida
The Institute of Scientific and Industrial Research, Osaka University, Osaka, Japan

*Address all correspondence to: yang@sanken.osaka-u.ac.jp

IntechOpen

© 2020 The Author(s). Licensee IntechOpen. This chapter is distributed under the terms of the Creative Commons Attribution License (<http://creativecommons.org/licenses/by/3.0>), which permits unrestricted use, distribution, and reproduction in any medium, provided the original work is properly cited. 

References

- [1] Migus A, Gauduel Y, Martin JL, Antonetti A. Excess electrons in liquid water: First evidence of a prehydrated state with femtosecond lifetime. *Physical Review Letters*. 1987;**58**:1559-1562. DOI: 10.1103/PhysRevLett.58.1559
- [2] Long FH, Lu H, Eisenthal KB. Femtosecond studies of the presolvated electron: An excited state of the solvated electron? *Physical Review Letters*. 1990; **64**:1469-1472. DOI: 10.1103/PhysRevLett.64.1469
- [3] Laenen R, Roth T, Laubereau A. Novel precursors of solvated electrons in water: Evidence for a charge transfer process. *Physical Review Letters*. 2000;**85**:50-53. DOI: 10.1103/PhysRevLett.85.50
- [4] Hong KM, Noolandi J. Solution of the Smoluchowski equation with a coulomb potential. I. General results. *The Journal of Chemical Physics*. 1987;**68**:5163-5171. DOI: 10.1063/1.435636
- [5] Tagawa S, Washio M, Kobayashi H, Katsumura Y, Tabata Y. Picosecond pulse radiolysis studies on geminate ion recombination in saturated hydrocarbon. *Radiation Physics and Chemistry*. 1983;**21**:45-52. DOI: 10.1016/0146-5724(83)90128-0
- [6] Tagawa S, Hayashi N, Yoshida Y, Washio M, Tabata Y. Pulse radiolysis studies on liquid alkanes and related polymers. *Radiation Physics and Chemistry*. 1989;**34**:503-511. DOI: 10.1016/1359-0197(89)90053-2
- [7] Yoshida Y, Tagawa S, Kobayashi H, Tabata Y. Study of geminate ion recombination in a solute-solvent system by using picosecond pulse radiolysis. *Radiation Physics and Chemistry*. 1987;**30**:83-87. DOI: 10.1016/1359-0197(87)90088-9
- [8] Yang J, Kondoh T, Norizawa K, Nagaishi R, Taguchi M, Takahashi K, et al. Picosecond pulse radiolysis: Dynamics of solvated electrons in ionic liquid and geminate ion recombination in liquid alkanes. *Radiation Physics and Chemistry*. 2008;**77**:1233-1238. DOI: 10.1016/j.radphyschem.2008.05.031
- [9] Kondoh T, Yang J, Norizawa K, Kan K, Yoshida Y. Femtosecond pulse radiolysis study on geminate ion recombination in n-dodecane. *Radiation Physics and Chemistry*. 2011;**80**: 286-290. DOI: 10.1016/j.radphyschem.2010.07.049
- [10] Kondoh T, Yang J, Norizawa K, Kan K, Kozawa T, Ogata A, et al. Femtosecond pulse radiolysis study of geminate ion recombination in biphenyl-dodecane solution. *Radiation Physics and Chemistry*. 2013;**84**:30-34. DOI: 10.1016/j.radphyschem.2012.06.051
- [11] Allen AO. *The Radiation Chemistry of Water and Aqueous Solutions*. Princeton, N.J.: Van Nostrand; 1961
- [12] Rodgers MAJ. Farhataziz, *Radiation Chemistry: Principles and Applications*. VCH: Weinheim; 1987
- [13] Hart EJ, Boag JW. Absorption spectrum of the hydrated electron in water and in aqueous solutions. *Journal of the American Chemical Society*. 1962; **84**:4090-4095. DOI: 10.1021/ja00880a025
- [14] Bronskill MJ, Taylor WB, Wolff RK, Hunt JW. Design and performance of a pulse radiolysis system capable of picosecond time resolution. *The Review of Scientific Instruments*. 1970;**41**: 333-340. DOI: 10.1063/1.1684511
- [15] Tabata Y, Kobayashi H, Washio M, Tagawa S, Yoshida Y. Pulse radiolysis with picosecond time resolution. *Radiation Physics and Chemistry*. 1985;

26:473-479. DOI: 10.1016/0146-5724(85)90195-5

[16] Kobayashi H, Tabata Y. A 20 ps time resolved pulse radiolysis using two linacs. *Nuclear Instruments and Methods: Section B*. 1985;10:1004-1006. DOI: 10.1016/0168-583X(85)90158-2

[17] Yoshida Y, Tagawa S, Washio M, Kobayashi H, Tabata Y. Picosecond pulse radiolysis on geminate ion recombination and formation of solute excited state in liquid cyclohexane. *Radiation Physics and Chemistry*. 1989;34:493-496. DOI: 10.1016/1359-0197(89)90051-9

[18] Yoshida Y, Ueda T, Kobayashi T, Shibata H, Tagawa S. Studies of geminate ion recombination and formation of excited states in liquid n-dodecane by means of a new picosecond pulse radiolysis system. *Nuclear Instruments and Methods A*. 1993;327:41-43. DOI: 10.1016/0168-9002(93)91405-C

[19] Yoshida Y, Mizutani Y, Kozawa T, Saeki A, Seki S, Tagawa S, et al. Development of laser-synchronized picosecond pulse radiolysis system. *Radiation Physics and Chemistry*. 2001;60:313-318. DOI: 10.1016/S0969-806X(00)00368-6

[20] Kozawa T, Mizutani Y, Miki M, Yamamoto M, Suemine S, Yoshida Y, et al. Development of subpicosecond pulse radiolysis system. *Nuclear Instruments and Methods: Section A*. 2000;440:251-253. DOI: 10.1016/S0168-9002(99)00997-3

[21] Wishart JF, Cook AR, Miller JR. The LEAF picosecond pulse radiolysis facility at Brookhaven National Laboratory. *The Review of Scientific Instruments*. 2004;75:4359-4365. DOI: 10.1063/1.1807004

[22] Muroya Y, Lin M, Han Z, Kumagai Y, Sakumi A, Ueda T, et al. Ultra-fast pulse radiolysis: A review of the recent system

progress and its application to study on initial yields and solvation processes of solvated electrons in various kinds of alcohols. *Radiation Physics and Chemistry*. 2008;77:1176-1182. DOI: 10.1016/S0969-806X(00)00367-4

[23] Aoki Y, Nkajyo T, Tsunemi A, Yang J, Okada Y, Yorozu M, et al. Performance of compact pulse radiolysis system using a photocathode RF gun. *Research on Chemical Intermediates*. 2001;27:689-697. DOI: 10.1163/15685670152621951

[24] Marignier J-L, Waele V, Monard H, Gobert F, Larbre J-P, Demarque A, et al. Time-resolved spectroscopy at the picosecond laser-triggered electron accelerator ELYSE. *Radiation Physics and Chemistry*. 2006;75:1024-1033. DOI: 10.1016/j.radphyschem.2005.10.020

[25] Kawaguchi M, Ushida K, Kashiwagi S, Kuroda R, Kuibayashi T, Kobayashi M, et al. Development of compact picosecond pulse radiolysis system. *Nuclear Instruments and Methods: Section B*. 2005;236:425-431. DOI: 10.1016/j.nimb.2005.04.012

[26] Yang J, Kan K, Naruse N, Yoshida Y, Tanimura K, Urakawa J. Femtosecond pulse radiolysis and femtosecond electron diffraction. *Nuclear Instruments and Methods in Physics Research A*. 2011;637:S24-S29. DOI: 10.1016/j.nima.2010.02.014

[27] Yang J, Kondoh T, Kan K, Yoshida Y. Ultrafast pulse radiolysis. *Nuclear Instruments and Methods in Physics Research A*. 2010;629:6-10. DOI: 10.1016/j.nima.2010.11.109

[28] Yang J, Kondoh T, Kan K, Kozawa T, Yoshida Y, Tagawa S. Femtosecond single electron bunch generation by rotating longitudinal bunch phase space in magnetic field. *Nuclear Instruments and Methods in Physics Research A*. 2006;556:52-56. DOI: 10.1016/j.nima.2005.10.115

- [29] Yang J, Kondoh T, Kozawa T, Yoshida Y, Tagawa S. Pulse radiolysis based on a femtosecond electron beam and a femtosecond laser light with double-pulse injection technique. *Radiation Physics and Chemistry*. 2006; **75**:1034-1040. DOI: 10.1016/j.radphyschem.2005.09.016
- [30] Oulianov DA, Crowell RA, Gosztola DJ, Shkrob IA, Korovyanko OJ, Rey-de-Castro RC. Ultrafast pulse radiolysis using a terawatt laser Wakefield accelerator. *Journal of Applied Physics*. 2007; **101**:053102. DOI: 10.1063/1.2696204
- [31] Yang J, Kondoh T, Yoshida A, Yoshida Y. Double-decker femtosecond electron beam accelerator for pulse radiolysis. *The Review of Scientific Instruments*. 2006; **77**:043302. DOI: 10.1063/1.2195090
- [32] Kan K, Kondoh T, Yang J, Ogata A, Norizawa K, Yoshida Y. Development of double-decker pulse radiolysis. *The Review of Scientific Instruments*. 2012; **83**:073302. DOI: 10.1063/1.4731652
- [33] Yang J, Kondoh T, Norizawa K, Yoshida Y, Tagawa S. Breaking time-resolution limits in pulse radiolysis. *Radiation Physics and Chemistry*. 2009; **78**:1164-1168. DOI: 10.1016/j.radphyschem.2009.07.017
- [34] Wishart JF, Rao BSM. *Recent Trends in Radiation Chemistry*. New Jersey: World Scientific Publishing Co. Pte. Ltd.; 2010
- [35] Yang J, Kondoh T, Yoshida Y, Tagawa S. Experimental studies of transverse and longitudinal beam dynamics in photoinjector. *Japanese Journal of Applied Physics*. 2005; **44**: 8702-8707. DOI: 10.1143/JJAP.44.8702
- [36] Yang J, Sakai F, Yorozu M, Okada Y, Yanagida T, Endo A. Experimental studies of emittance growth and energy spread in a photocathode RF gun. *Nuclear Instruments and Methods in Physics Research A*. 2002; **491**:15-22. DOI: 10.1016/S0168-9002(02)01181-6
- [37] Sakai F, Yang J, Yorozu M, Okada Y, Yanagida T, Endo A. Stable high-brightness electron beam system with a photocathode RF gun for short pulse X-ray generation by Thomson scattering. *Japanese Journal of Applied Physics*. 2002; **41**:1589-1594. DOI: 10.1143/JJAP.41.1589
- [38] Yang J, Sakai F, Yanagida T, Yorozu M, Okada Y, Takasago K, et al. Low-emittance electron-beam generation with laser pulse shaping in photocathode radio-frequency gun. *Journal of Applied Physics*. 2002; **92**:1608-1612. DOI: 10.1063/1.1487457
- [39] Nozawa I, Kan K, Yang J, Ogata A, Kondoh T, Gohdo M, et al. Measurement of < 20 fs bunch length using coherent transition radiation. *Physical Review Accelerators and Beams*. 2014; **17**:072803. DOI: 10.1103/PhysRevSTAB.17.072803
- [40] Yang J, Yoshida Y. Ultrafast pulse radiolysis for observation of short-lived intermediate species in radiation chemistry. *Radioisotopes*. 2017; **66**(10): 395-406. DOI: 10.3769/radioisotopes.66.395
- [41] Elles CG, Jailaubekov AE, Crowell RA, Bradforth SE. Excitation-energy dependence of the mechanism for two-photon ionization of liquid H₂O and D₂O from 8.3 to 12.4 eV. *The Journal of Chemical Physics*. 2006; **125**:044515. DOI: 10.1063/1.2217738
- [42] Pimblott SM, Laverne JA, Bartels DM, Jonah CD. Reconciliation of transient absorption and chemically scavenged yields of the hydrated electron in radiolysis. *The Journal of Physical Chemistry*. 1996; **100**: 9412-9415. DOI: 10.1021/jp960816f